Single-Facet Dominant Anatase TiO_2 (101) and (001) Model Catalysts to Elucidate the Active Sites for Alkanol Dehydration

Fan Lin,[†,♯] Yuan Chen,[†,♯] Lu Zhang,[†, ♯] Donghai Mei,[†] Libor Kovarik,[†] Berlin Sudduth,[‡] Huamin Wang,[,†] Feng Gao,*[,†] Yong Wang*[,†,‡]*

[†] Institute for Integrated Catalysis, Pacific Northwest National Laboratory, Richland, Washington 99354, USA

[‡] The Gene and Linda Voiland School of Chemical Engineering and Bioengineering, Washington State University, Pullman, Washington 99164, USA

♯ These authors contributed equally

* To whom correspondence should be addressed

H. Wang (huamin.wang@pnnl.gov), F. Gao (feng.gao@pnnl.gov) and Y. Wang (yong.wang@pnnl.gov)

ABSTRACT

Alkanol dehydration on Lewis acid-base pairs of transition metal oxide catalysts is a reaction of importance in oxygen removal from biomass-derived feedstocks and their conversion to chemicals in general. However, catalysts with a high degree of structural heterogeneity, such as commercial TiO_2 powders, are not well-suited to establish rigorous structure-function relationships at an atomic level. Here, we provide compelling evidence for the effects of surface orientation of TiO_2 catalyst on elimination reactions of alcohols. Two anatase titania model catalysts, with preferential exposure of (101) and (001) facets, were synthesized and studied for 2-propanol dehydration using kinetic, isotopic, microscopic, and spectroscopic measurements, coupled with DFT calculations. Surface Lewis acid sites were found to be active for 2-propanol dehydration and (101) facets are more reactive than (001) facets under the reaction conditions studied. On both anatase surfaces, 2-propanol was found to dehydrate via concerted E2 elimination pathways, but with different initial states and thus also different intrinsic activation barriers. Molecular 2-propanol dehydration dominates on TiO_2 (101) while on TiO_2 (001), 2-propanol simultaneously converts to more stable 2-propoxide before dehydration, which then requires higher activation energies for E2 elimination.

KEYWORDS: TiO_2, dehydration, facet, E2 elimination, DFT, Lewis acid base

TABLE OF CONTENTS (TOC)

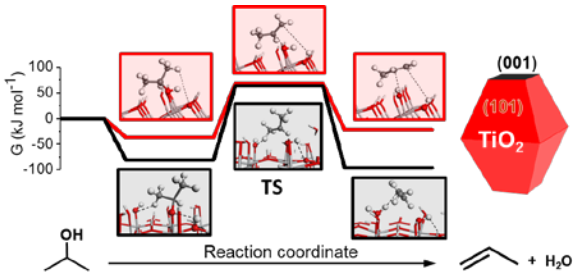

INTRODUCTION

The catalytic dehydration of alcohols represents an important class of oxygen-removal reactions in the transformation of biomass-derived molecules into fuels and chemicals.[1] Oxide-based solid acid catalysts are widely used to catalyze this reaction, because of their high efficiency and their low toxicity and cost.[2,3] Understanding the active sites of metal oxides remains crucial in the design of more effective catalysts for the dehydration processes. Catalysts with a high degree of structural heterogeneity, such as commercial TiO_2 powders, are not well-suited to establish rigorous structure-function relationships at an atomic level. Nanomaterials with well-controlled surface structures that expose predominant (or even single) facets circumvent these obstacles. In the present study, we choose two anatase TiO_2 with preferential exposure of (101) and (001) facets as model oxide catalysts, which have significantly different surface energies (0.44 and 0.90 J m^{-2} for (101) and (001), respectively),[4,5] to examine the nature of the required active sites and the elementary steps involved in these reactions.

Recently, anatase TiO_2 nanocrystals with dominant facets have received significant attention in thermochemical and photochemical catalysis.[6-8] For example, Gordon et al.[9] reported the use of TiF_4 to engineer and control the exposure of (101) and (001) facets in anatase TiO_2 nanocrystals. Their results showed that the (101)-dominant catalysts exhibited higher catalytic activity per unit weight than (001)-dominant catalysts for the photocatalytic evolution of H_2 from H_2O. In other applications, such as the photochemical degradation of organic contaminants, TiO_2 (001) facets have been reported to be more efficient than TiO_2 (101) facets, plausibly because of their higher surface energy.[10-14] Most of the applications to date have focused on the single facet anatase model catalysts for photocatalytic reactions, but some previous studies examined the use of these model catalysts for thermocatalytic reactions.[15,16]

In all cases, the use of these model catalysts to examine the effects of surface structure on surface reactions requires stringent cleanliness of all exposed surfaces. This requirement is not often met

because heteroatoms are typically required for the synthesis of facet-dominant materials; these heteroatoms include F^- (from HF or TiF_4 as the directing or capping agents) or Na^+ and K^+ from the bases used (NaOH and KOH).[17,18] The presence of these heteroatoms can strongly influence the electronic and surface properties of a catalyst surface and their post-synthesis removal can lead to catalyst structural collapse,[19] resulting in the assignment of ambiguous or incorrect catalytic properties to specific surface exposures. We will show below in the experimental section how such heteroatoms are avoided for the current study.

Previous work[3,20,21] have studied the mechanism of alcohol dehydration on metal oxides, including TiO_2, and proposed an E2 elimination mechanism, in which Lewis acid sites (metal cations, e.g., Al^{3+} and Ti^{4+}) act as the active centers when paired with vicinal basic surface O-atoms or OH groups. Such a proposal differs from the conventional treatment of surface OH groups as Brønsted acids. Larmier et al.[22] accepted this mechanistic proposal in their studies of alcohol dehydration on alumina and considered acid-base proximity, instead of the nature of the basic site center (OH or O), to be the critical determinant of reactivity. Other studies of alcohol dehydration catalysis on TiO_2, ZrO_2 or TiO_2-ZrO_2 mixed oxide, however, attribute reactivity to differences in the number of Brønsted acid sites, which were more abundant on TiO_2-ZrO_2.[23,24] On classical Brønsted acid catalysts (e.g., H-ZSM-5), Lercher and coworkers[1] suggested that 1-propanol dehydration was catalyzed by a Brønsted acid site involving both dimer and monomer intermediates. In studying alkanol dehydration over another classic Brønsted acid catalyst that contains no Lewis acidity, i.e., heteropolyacids, Iglesia and coworkers[25,26] discovered that detailed pathways depend critically on the acid strength and the chain length of the alkanols. These studies indicate that the nature of alcohol dehydration active sites and reaction routes on metal oxides, especially ones containing both Brønsted and Lewis acid sites, remain uncertain and the ultimate discrimination among different hypotheses would be challenging on materials containing both types of acid sites as well as Lewis acid/base pairs.

Here, we report the use of low-index facet-selective anatase TiO_2 as model catalysts for the thermocatalytic dehydration of 2-propanol. To the best of our knowledge, previous studies have not investigated the influence of anatase facets on 2-propanol dehydration reactivity. Anatase TiO_2 nanocrystals with dominant exposures of (101) and (001) were prepared using fluoride-free hydrothermal techniques. These model catalysts were evaluated for 2-propanol dehydration using kinetic, isotopic, microscopic and spectroscopic techniques coupled with DFT calculations. It was found that Lewis acid is the active site. On both catalyst surfaces, 2-propanol dehydration appears to follow a concerted E2 elimination pathway with the β C-H bond cleavage governing the reaction rate. However, two different initial states are involved prior to 2-propanol dehydration. Molecular 2-propanol adsorption dominates on (101) while on (001), 2-propanol readily dissociates to form more stable 2-propoxide, requiring higher activation energy for E2 elimination.

METHODS AND MATERIALS

Catalyst Preparation. Facet-selective titania anatase nanocrystals were synthesized using hydrothermal techniques involving two steps: precursor preparation and crystal growth. The catalyst precursor was first prepared by heating the mixture of KOH (Sigma-Aldrich, ≥ 85wt%)solution and P25 (Aldrich, nanopowder, 21 nm in diameter, ≥ 99.5wt%) at 473 K and then dried at 353 K overnight.[38] TiO_2 (101) was prepared by adding 0.2 g of precursor to 180 cm^3 ultrapure water and sonicating the mixture for 30 min. The pH of the mixture was then adjusted to 5.0 by adding 0.1 M HNO_3 (Sigma-Aldrich, ACS reagent, 70%) drop-wise. The resulting synthesis solution was sealed into a 125 cm^3 Teflon-lined stainless-steel autoclave (~60 cm^3 in each) and maintained at 473 K for 48 h. TiO_2 (001) was prepared by adding 0.25 g of precursor to 250 cm^3 ultrapure water and sonicating for 45 min. The preferential growth of (001) facet was induced by adding 45 g of urea (Sigma-Aldrich, ACS reagent) to the solution as a capping agent. The pH of the mixture was adjusted to 13 by gradually adding about 40 cm^3 of KOH (0.3 M). The

resulting solution was again sealed into an autoclave and heated at 473 K for 20 h. The as-synthesized catalysts were washed 5 times using ultrapure water, separated by centrifugation, and dried in air at 353 K overnight. The samples were then treated in static air at 823 K for 4 h for impurity removal and structural stabilization. In short, to prepare model catalysts with the highest possible purity, here we used the fluoride-free hydrothermal techniques with urea as the capping agent, which can be readily removed by simple calcination. We also thoroughly washed the synthesized materials for removal of K^+ ions. XPS analysis demonstrated that for all of the catalysts studied here, surface area K/Ti atomic concentrations were $\leq 0.3\%$, corresponding to surface K coverages less than ~0.02 K/nm^2. Further washing had no influence on dehydration activities of these catalysts.

Catalyst Characterization. Surface area measurements were conducted on a QuantaChrome Autosorb-6 using N_2 adsorption isotherms and BET analysis methods. Samples were degassed in vacuum at 423 K for 4 h before adsorption measurements. X-ray diffractograms were collected with a Philips PW3040/00 X'Pert MPD system equipped with a Cu K-α source ($\lambda = 1.5406$ Å). Diffractograms were analyzed using JADE software (Materials Data, Livermore, CA) and crystallite sizes determined using the Scherrer equation.

Scanning electron micrographs were acquired using an FEI Helios 600 NanoLab FIB-SEM. TEM was carried out using a JEOL JEM 2010 system operated at 200 keV. The TEM specimens were prepared by dispersing calcined TiO_2 samples in ethanol and depositing the suspension onto a lacey carbon-coated copper grid.

X-ray photoelectron spectra were measured with a Physical Electronics Quantera Scanning X-Ray Microprobe using a focused monochromatic Al Kα X-ray (1486.7 eV) source for excitation and a spherical section analyzer. The X-ray beam is incident normal to the sample and the photoelectron detector is placed at 45° off-normal. High-resolution spectra were collected using a pass-energy of 69.0 eV with a step size of 0.125 eV.

NH_3-TPD was performed using a plug-flow reactor cell equipped with an online MKS 2030 FTIR analyzer. The calcined catalyst (100 mg) was treated at 773 K in He at a flow rate of 300 cm^3 min^{-1} and cooled to 373 K. A stream of NH_3 (300 ppm) in He was introduced for 30 min to saturate the catalyst surface. The sample was then purged with He at 373 K for at least 3 h to remove physisorbed NH_3. NH_3 desorption was then carried out by heating the sample from 373 to 873 K at 10 K min^{-1} and holding at 873 K until desorption of NH_3 was not detectable. The NH_3 concentration in the effluent was recorded as a function of temperature. NH_3 desorption was then quantified to estimate the acid site density for each catalyst. We note that this quantification will be used in the following to quantify 2-propanol dehydration rates.

The type of acid sites in these samples was probed using DRIFT spectra of bound pyridine obtained with a Bruker Tensor 27 FTIR spectrometer equipped with an in situ reaction chamber (Harrick Scientific Products Inc.). Around 50 mg of sample was loosely packed into the reaction chamber to form a smooth flat surface and treated at 773 K in 10% O_2/He for 30 min, cooled down to 373 K, and purged with He for another 1 h before pyridine vapor was introduced using a bubbler and He as the carrier gas until the catalyst surface was saturated with pyridine (pyridine IR features maintained invariant with time). The sample was flushed with 100 $cm^3 \cdot min^{-1}$ He for 1 h to remove the physisorbed pyridine. Samples were then heated to different target temperatures (373, 503, 533, 573, 773 K) in flowing He and held for 20 min before IR spectra were acquired. Spectral backgrounds were subtracted using data for samples at 373 K after pretreatment, before exposure to pyridine.

2-propanol Dehydration Tests. 2-propanol dehydration was tested using two methods: (1) temperature-programmed desorption (TPD) in a Micromeritics AutoChem II 2920 Chemisorption Analyzer with an online QMS (Quadra 220) and (2) isothermal steady-state kinetic studies in a quartz reactor with plug-flow hydrodynamics. The TPD measurements used 100 mg of samples placed in a quartz reactor tube and treated in flowing He at 100 cm^3/min at 573 K or 1 h. After

cooling down to 373 K, 2-propanol was introduced by flowing 100 cm^3/min He through a bubbler containing liquid 2-propanol at 333K until samples were saturated (no change of 2-propanol concentration in the effluent gas). The sample was then flushed with 100 cm^3/min He for 1 h in order to remove weakly-adsorbed 2-propanol. The sample temperature was then increased from 373 to 873 K at 10 K/min in a 100 cm^3/min 5%Ar/He flow. All species in the effluent were analyzed by an on-line mass spectrometry. Ar was used as an internal standard for mass spectrometric quantitation.

Steady-state rate measurements were carried out by introducing 2-propanol into He flow with a syringe pump. Titania catalysts (25 mg) were diluted with 2.5 g of inert SiC, which were treated in 20% O_2/He at 573 K for 1 h to eliminate the carbonaceous contamination before introducing reactants at 2 kPa partial pressure. Rates were measured at temperatures between 503 and 533 K (10 K increments) with varied space velocities to maintain conversions below < 5%. 2-propanol pressure effects on rates were examined at 0.3 to 4 kPa. We have conducted pretreatment of the catalysts at temperatures of 573 K and 773 K, respectively, and found that the pretreatment temperature did not affect the measured rates. In titration experiments during reaction, 2,6-di-tert-butylpyridine (Sigma Aldrich, 97%) was introduced with 2-propanol (C_3H_8O/2,6-di-tert-butylpyridine molar ratio = 1000; 2 kPa 2-propanol, 26.2 $mol \cdot min^{-1} \cdot g^{-1}_{cat}$.). Kinetic isotope effects were conducted using deuterated 2-propanol (CH_3-CD(OH)-CH_3, CD_3-CH(OH)-CD_3, CD_3-CD(OD)-CD_3) at 533 K and 2 kPa of each molecule. The reaction products were analyzed using an Agilent 7890A GC equipped with a flame-ionization detector using a HP-5 (30 m × 0.25 mm × 0.50 μm) column. The reaction turnover rates were calculated by normalizing the reaction rates by the total number of Lewis acid sites determined with NH_3-TPD and pyridine-IR.

DRIFTS. To gain details on 2-propanol chemisorption characteristics on the model surfaces, especially to mimic surface species and coverages under steady-state reaction conditions for

theoretical simulations, DRIFTS experiments were conducted. DRIFT spectra for 2-propanol adsorption on the TiO_2 model catalysts were collected with a Nicolet, Magna 6700 FTIR spectrometer equipped with a liquid nitrogen-cooled MCT detector and operated at 4 cm^{-1} resolution, and each spectrum was an average of 128 scans. Briefly, ~50 mg of finely ground TiO_2 (101) or (001) sample was loaded in the reaction cell (Harrick Scientific Products, Inc.). The sample was then ramped to 773 K (10K/min) for in-situ pretreatment under He flow (50 ml/min). After holding at 773 K for 1 h, the sample was stepwise cooled to 373 K at 50-K intermission in the same gas flow. 2-propanol was introduced into the reaction cell by flowing He (~5 ml/min) through a 2-propanol filled bubble generator at 373 K until saturation (i.e., signal intensity became invariant with time). Physisorbed 2-propanol was thereafter removed by He purging for 1 h. The desorption process was monitored by stepwise heating the 2-propanol-chemisorbed sample with a ramping rate of 10 K/min at 10 K intermissions. At each target temperature, DRIFT spectrum was acquired and further analyzed using KBr background collected at the same temperature.

Density Functional Theory Calculations. First principles periodic DFT calculations were performed using the CP2K code[39]. Core electrons were represented with norm-conserving Goedecker-Teter-Hutter pseudopotentials[40-42] and the valence electron wavefunctions were expanded in a double-zeta basis set with polarization functions[43] along with an auxiliary plane wave basis set with an energy cutoff of 360 Ry. The generalized gradient approximation exchange-correlation functional of Perdew, Burke, and Enzerhof (PBE)[44] was used. Excess electrons associated with the Ti 3d orbitals were treated using DFT+U method with a U value of 7.0 eV as suggested before.[45] The maximum coordinate change of 3.0×10^{-4} bohr was achieved when the maximum force convergence criteria of 4.5×10^{-5} Hartree/bohr was used in the geometry optimization. Each reaction state configuration was optimized with the Broyden-Fletcher-Goldfarb-Shanno (BGFS) algorithm with self-consistent field (SCF) convergence criteria of 1.0×10^{-8} au. The van der Waals (vdW) dispersion interactions between adsorbates were described using the DFT-D3 scheme[46] with an empirical damped potential term.

Transition states of elementary steps were located using the climbing image nudged elastic bands (CI-NEB) method[47,48] with seven intermediate images along the reaction pathway between initial and final states.

Anatase TiO_2(101) surfaces contain equal numbers of five-fold (Ti_{5c}) and six-fold (Ti_{6c}) coordinated Ti atoms linked with two types of oxygen atoms in two-fold (O_{2c}) and three-fold (O_{3c}) coordinations. Anatase TiO_2(101) surfaces are represented here by a periodic p(3×3) super cell with the simulation box parameters of 1.08858×1.52501×2.69842 nm^3 and α= 68.2678°, $\beta=\gamma=90°$ (8 TiO_2 units on the surface). Anatase TiO_2(001) surfaces contain only two-fold bridging oxygen atoms (O_{2c}) and five-fold Ti atoms (Ti_{5c}). Anatase TiO_2(001) surface are represented here by a periodic p(3×3) super cell with the simulation box parameters of 1.13280×1.13280×2.29113 nm^3 and $\alpha=\beta=\gamma=90°$ (9 TiO_2 units on the surface). On both (101) and (001) surfaces, only Ti_{5c} sites act as Lewis acid sites. To validate the accuracy of our model surfaces, different thicknesses of anatase (001) and (101) surface slabs with 4 to 8 atomic layers were tested. Our calculated adsorption energies of 2-propanol suggest that both surface slabs with four atomic layers are accurate enough for adsorption and further reaction pathway investigation.

The Gibbs free energies (ΔG_{ad}) for 2-propanol and water adsorption on anatase (001) and (101) surfaces were calculated using[49]

$$\Delta G_{\mathrm{ad}} = \frac{G_{\mathrm{TiO_2(hkl)}+n\cdot\mathrm{adsorbate}} - (G_{\mathrm{TiO_2(hkl)}} + n\cdot G_{\mathrm{adsorbate}})}{n} \qquad (3)$$

where $G_{\mathrm{TiO_2(hkl)}+n\cdot\mathrm{adsorbate}}$ is the Gibbs free energy of the anatase surface (hkl) (hkl=101 or 001) with n adsorbate molecules (2-propanol or water); $G_{\mathrm{TiO_2(hkl)}}$ is the Gibbs free energy of the clean anatase surface and $G_{\mathrm{adsorbate}}$ is the Gibbs free energy of gaseous molecules. All Gibbs free energies associated with surfaces were calculated using the standard thermodynamic method. The vibrational entropy and zero-point energy correction (ZPEC) were calculated with vibrational frequencies where the adsorbate and surface atoms directly connected with the adsorbate are included. The $G_{\mathrm{adsorbate}}$ was calculated as[49]

$$G_{\text{adsorbate}} = H^0_{\text{adsorbate}} - TS^0_{\text{adsorbate}} + RT\ln\left(\frac{P_{\text{adsorbate}}}{P^0_{\text{adsorbate}}}\right) \quad (4)$$

where H^0 and S^0 represent standard condition (T=298.15 K; P=1 bar) enthalpy and entropy; T and $P_{\text{adsorbate}}$ represent experimental reaction temperature and pressure. The calculated $G_{\text{adsorbate}}$ results with co-existed water and 2-propanol are given in Supplementary Tables 1 and 2, suggesting that only one 2-propanol on hydroxylated TiO_2 (101) and (001) surfaces is most stable.

To account for important entropy (ΔS) and ZPEC contributions to the 2-propanol dehydration, both Gibbs free energy (ΔG) and enthalpy (ΔH) changes along the reaction pathways were calculated using statistical thermodynamic method, which had been discussed in detail in previous work:[1,50,51]

$$\Delta G = \Delta H - T\Delta S \quad (5)$$

$$\Delta H = \Delta U_{\text{trans}} + \Delta U_{\text{rot}} + \Delta U_{\text{vib}} + \Delta(ZPE) + \Delta H_{\text{elec}} \quad (6)$$

$$\Delta S = \Delta S_{\text{trans}} + \Delta S_{\text{rot}} + \Delta S_{\text{vib}} \quad (7)$$

where the translational, rotational, and vibrational contributions to the internal energy (ΔU) and ZPE were given in the Supplemental Information. The electronic term (ΔH_{elec}) was directly derived from DFT calculations. The activation barrier ($\Delta H^{\ddagger}$) and Gibbs energy of activation ($\Delta G^{\ddagger}$) for each elementary reaction step then were similarly obtained as the corresponding enthalpy and Gibbs free energy difference between the initial and the transition states.

RESULTS

Structural and Physicochemical Properties of Anatase TiO_2 (101) and TiO_2 (001) Model Catalysts. The hydrothermal synthesis conditions used and the physicochemical properties of anatase TiO_2 (101) and (001) are shown in Table 1. TiO_2 (101) exhibits higher surface areas than TiO_2 (001), consistent with the smaller crystallites evident from SEM images and diffractograms (Supplementary Figure 1). SEM and TEM micrographs of anatase TiO_2 (101) and (001) samples

are shown in Figure 1. TiO_2 (101) sample has particles of uniform size (80-125 nm in length; 30-50 nm in width) and bipyramidal shape. About 90% of the exposed surfaces on this sample have the interplanar spacing of 0.346 nm (Figure 1 (c)) characteristic of (101) facets with the rest consisting of (001) facets at corners and high-index facets on the edges. The TiO_2 (001) model catalyst, in contrast, shows square platelets structures that are 150-200 nm in length and 40-60 nm in thickness. The interplanar spacing (0.472 nm) indicates the predominant presence of (001) facets (Figure 1 (f)). These (001) facets represent about 76% surface of the TiO_2 (001) model catalyst; the exposed facets at edges are mostly (101), but also include some high-index facets. These results show that $(NH_4)_2CO$ acts as a capping agent that stabilizes (001) surfaces, thus allowing preferential crystal growth along the (101) orientation and leading to the predominant exposure of (001) facets at crystal surfaces.

Table 1. Hydrothermal synthesis conditions and physochemical properties for anatase TiO_2 catalysts

Catalysts		TiO_2 (101)	TiO_2 (001)
pH		<5	>13
T (K)		473	473
Time (h)		48	24
Capping agent		-	$(NH_2)_2CO$
Surface area (m^2 g^{-1})		24.5	13.5
Facet fractions (%)	f(101)	90	24
	f(001)	10	76
Acid site density (nm^{-2})	Total[a]	1.14	0.72
	Lewis[b]	0.99	0.72
	Brønsted[b]	0.15	0

[a] Total acid site density was measured by NH_3-TPD; [b] The respective densities of Brønsted and Lewis acid sites were estimated based on their relative ratio (determined by pyridine-IR) and the total acid site density (measured by NH_3-TPD).

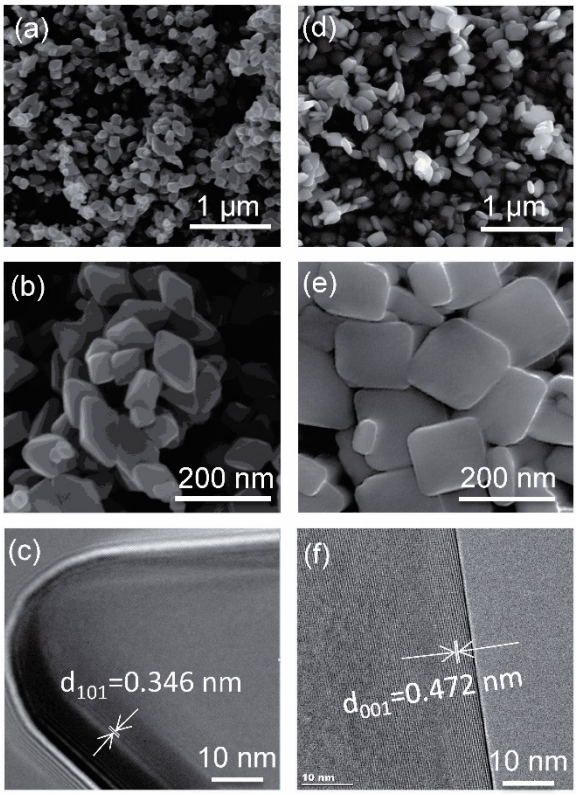

Figure 1. SEM and TEM micrographs of anatase titania nanocrystals model catalysts. (a)-(b) SEM micrographs of TiO_2 (101), (c) HR-TEM micrograph of TiO_2 (101) facet, (d)-(e) SEM micrographs of TiO_2 (001), and (f) HR-TEM micrograph of TiO_2 (001) facet.

The diffractograms for these two samples (Supplementary Figure 1) do not show lines for rutile or brookite TiO_2 phases but only anatase phase (most intense lines located at 25.3°, 37.8°, 48.1°, 53.9°, 55.1°, 62.7°, 68.8°, 70.4°, and 76.1° corresponding to the (101), (001), (100), (105), (211), (102), (116), (220), and (215) anatase crystal planes). Mean crystallite diameters obtained from diffraction lines using the Scherrer equation were 27 and 68 nm for (101) and (001) samples, respectively, calculated using the most intensive reflection at 25.3°. XPS spectra for these (101) and (001) samples (Supplementary Figure 2) show only Ti and O lines, without detectable K, N, and C impurities that may have resulted from synthesis residues. A detailed analysis of the Ti_{2p} and O_{1s} regions (Supplementary Figures 2(b) and 2(c)) shows identical features for $Ti_{2p(1/2)}$ at 464.4 eV

and for $Ti_{2p(2/3)}$ at 458.6 eV on the two samples, consistent with reported Ti_{2p} binding energies for anatase TiO_2[27].

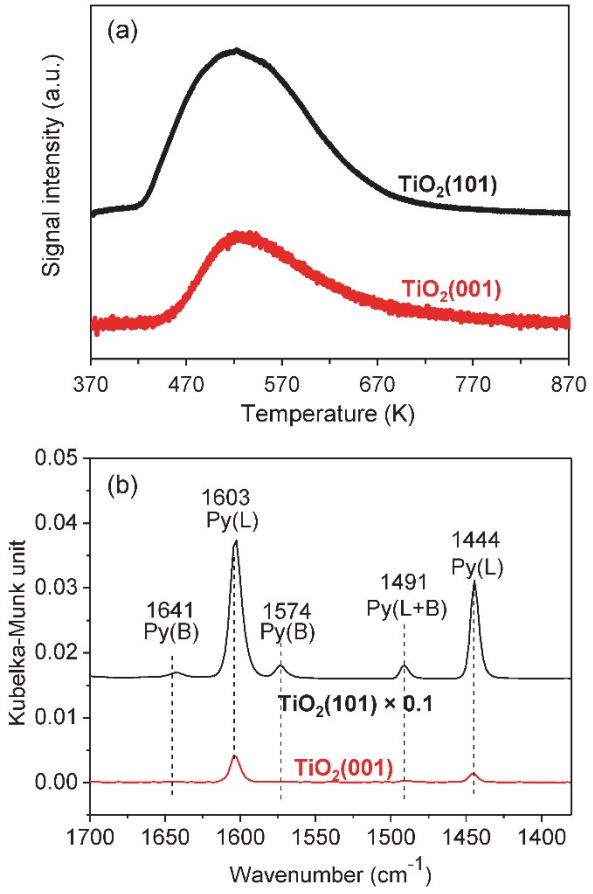

Figure 2. Acidity of the two catalysts. (a) NH_3-TPD profiles and (b) DRIFTS spectra (in Kubelka-Munk unit) of pyridine adsorption at 533 K for TiO_2 (101) and TiO_2 (001) catalysts.

Ammonia desorption profiles were used to measure the total number of the acid sites (including Brønsted and Lewis acid sites) on both samples (Figure 2(a)). Ammonia desorbs from both samples in a broad feature centered at ~533 K. Readsorption processes and the uncertain strength of Brønsted and Lewis acid sites preclude any assignments of this feature to specific types of these acid sites. Such data can therefore be used only to count the total number of acid sites in each sample. TiO_2 (101) shows a higher density of acid sites (1.14 sites nm^{-2}) than TiO_2 (001) (0.72 sites nm^{-2}) as shown in Table 1.

The type of acid sites on these samples was examined by assigning the infrared bands for pyridine bound to Lewis (Py(L)) and Brønsted (Py(B)) acid sites at 533K (Figure 2(b)). Anatase TiO_2(101) shows bands for Lewis (0.99 sites/nm^2) and Brønsted (0.15 sites/nm^2) acid sites corresponding to a 6.6:1 ratio based on band intensities (band 1444 cm^{-1} for Py(L) and 1574 cm^{-1} for Py(B), respectively) and the ratio of their molar extinction coefficients ($\varepsilon_{Py(B)}/\varepsilon_{Py(L)}$=0.75 [28]). In contrast, the pyridine spectra on TiO_2 (001) showed negligible adsorption on Brønsted acid sites (1574 cm^{-1}). The stability of bound pyridine on both samples was probed from spectra obtained as a function of temperature (273 K-673 K, Supplementary Figure 3), which indicates that Lewis acid sites on (101) are stronger than on (001).

2-Propanol Dehydration. The desorption and reaction rates of bound 2-propanol were examined as a function of temperature (TPD) and the evolution profiles for propylene and H_2O are shown in Figures 3(a) and 3(b), respectively. Figure 3(a) (propylene, 41 amu) shows a sharp single feature centered at 533 K on TiO_2(101); this feature is less intense and slightly shifts to 558 K on TiO_2(001). The H_2O evolution profiles (Figure 3(b); 18 amu) are more complex. TiO_2(101) shows two features at low temperatures (473 and ~533 K) and one at higher temperature (703 K). The 533 K feature coincides with the evolution of propylene. In contrast to TiO_2(101), the low-temperature desorption states on TiO_2(001) are much weaker (almost unresolved), yet the high-temperature state becomes much stronger. Apparently, TiO_2(101) is more reactive and H_2O adsorbs more strongly on TiO_2(001).

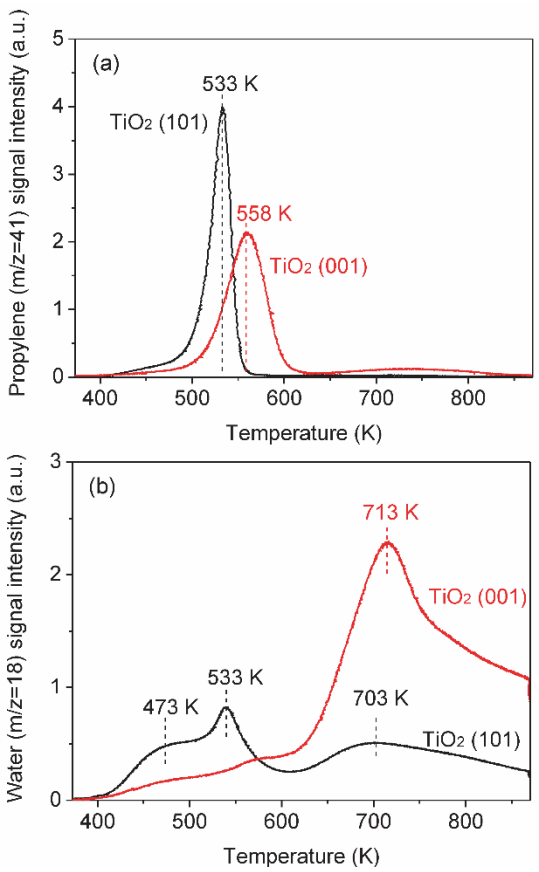

Figure 3. Temperature-programmed desorption of isopropanol**.** (a) Propylene (m/z = 41) and (b) H_2O (m/z = 18) desorption profiles in temperature-programmed desorption of isopropanol on TiO_2 (101) and TiO_2 (001) catalysts (signal intensities were normalized to per Lewis acid site basis).

Steady-state 2-propanol dehydration rates were measured at 0.3-4.0 kPa 2-propanol and from 503 K to 533 K at conversions below 5%. Propylene was formed at >99.8% selectivity with traces of diisopropyl ether (<0.2%) but no detectable formation of acetone (from dehydrogenation reactions). The dominance of 2-propanol dehydration over dehydrogenation on anatase TiO_2 in an inert carrier gas is consistent with previous reports.[20,21,29] In contrast, Rekoske et al.[30] reported higher selectivities for the dehydrogenation pathway during the steady state 2-propanol reaction on anatase TiO_2 than we observed in this work, probably because of somewhat different conditions applied in their work (e.g., commercial anatase TiO_2, higher oxidation pretreatment temperature). The fact that TiO_2 (001), which contains only Lewis acid sites, is active suggests that Lewis acids

act as the active sites. To further confirm this, we used 2,6-di-tert-butyl pyridine (2,6-DBPD) which selectively and irreversibly titrates Brønsted acid sites[31] and would therefore suppress any contributions to dehydration rates from such sites. On both catalysts dehydration rates were unaffected by the presence of 2,6-DBPD in the 2-propanol reactants (Supplementary Figure 4). This result is anticipated for TiO_2 (001) since no Brønsted acidity was measured from pyridine adsorption FTIR (Figure 2 (b)). For TiO_2 (101) that contains both Lewis and Brønsted acid sites, this finding demonstrates that the Brønsted acid sites on TiO_2 (101) do not catalyze 2-propanol dehydration. Since Brønsted acid sites on other oxides, e.g., alumina, do catalyze alkanol dehydration, the result found here indicates that Brønsted acid sites on TiO_2 (101) are too weak to catalyze the target dehydration reaction, and the Lewis acid sites are the active sites for 2-propanol dehydration. Therefore, the turnover rates were calculated by normalizing the reaction rates by the total number of Lewis acid sites.

The kinetic effects of 2-propanol partial pressure on dehydration turnover rates on TiO_2(101) and TiO_2(001) are shown in Figure 4. On both samples, rates increase monotonically with reactant pressure and then reach constant values at high 2-propanol partial pressures. These trends are accurately described by a Langmuir-Hinshelwood mechanism, which states that the rate of a heterogeneous reaction is controlled by the reaction of the adsorbed molecules, and that all adsorption and desorption are in equilibrium. By assuming a quasi-equilibrium for 2-propanol adsorption/desorption and water adsorption/desorption and elimination of water from bound 2-propanol-dervied intermediates as the rate-limiting step, the reaction mechanism can be described by the following equation,

$$r = \frac{k_2 K_1 [C_3H_8O]}{1 + K_1 [C_3H_8O] + K_3 [H_2O]} \qquad (1)$$

where [C_3H_8O] and [H_2O] denote the pressures of 2-propanol and water, respectively; K_1 is the 2-propanol adsorption equilibrium constant; K_3 is the water adsorption equilibrium constant, and k_2 denotes the rate constant for water elimination from bound 2-propanol-derived intermediates.

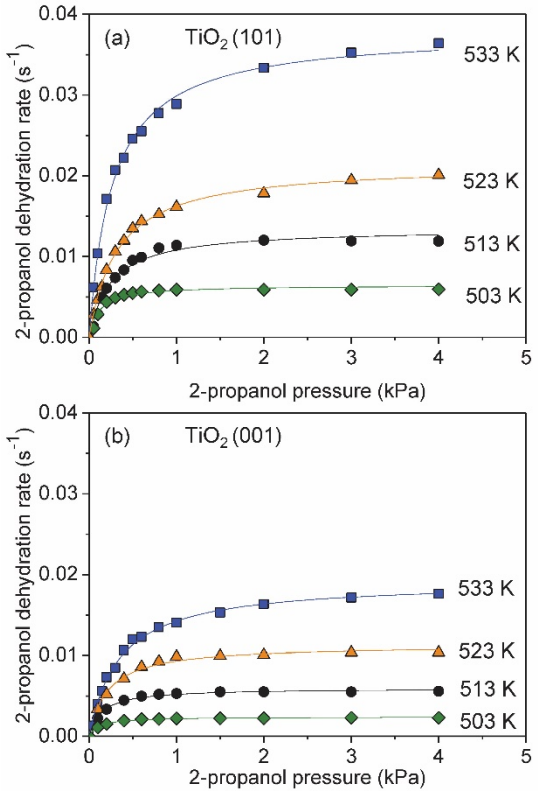

Figure 4. Steady-state 2-propanol dehydration kinetics. Isopropanol dehydration rate as a function of isopropanol partial pressure (0.3-4 kPa) for (a) TiO_2 (101) and (b) TiO_2 (001) at 533 K (■), 523 K (▲), 513 K (●), and 503 K(♦).

This reaction mechanism proposal with rate-determining step being surface dehydration is in agreement with kinetic isotope effect (KIE) measurements. Partial deuterium-substituted 2-propanol at alpha (CH_3-CD(OH)-CH_3) and beta positions (CD_3-CH(OH)-CD_3) and fully-deuterated CD_3-CD(OD)-CD_3 were used to compare with un-substituted 2-propanol. The KIE values for each D-substituted 2-propanol are listed in Table 2. Note that in these measurements, a 2-propanol partial pressure of 2 kPa was used. As indicated by Figure 4, this

pressure allows the measurements of k_2 values with reasonable accuracy. For both TiO_2(101) and (001) catalysts, deuterium-substitution in the alpha position exhibits no effect on 2-propanol reactivity. In contrast, beta- and fully-substituted 2-propanol exhibits comparable KIE values of ~1.6 for both catalysts, indicating that cleavage of the beta C-H(D) bond is kinetically relevant for both catalysts. The similarity in KIE indicates that the two catalysts possess similar lateness of the transition state.

Table 2. Kinetic isotope effects for deuterium-substituted 2-propanol dehydration on TiO_2 (101) and (001) catalysts

KIE	$CH_3CD(OH)CH_3$	$CD_3CH(OH)CD_3$	$CD_3CD(OD)CD_3$
TiO_2 (101)	1.0	1.6	1.6
TiO_2 (001)	1.0	1.7	1.7

Reaction conditions: 533 K, 2 kPa 2-propanols.

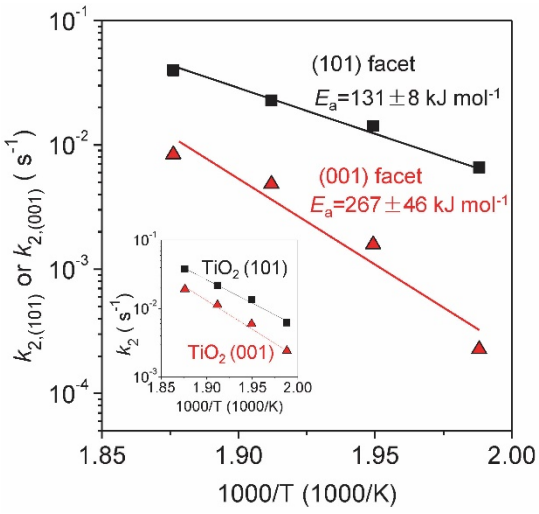

Figure 5. Arrhenius plots of the rate constants for isopropanol dehydration ($k_{2,(101)}$ or $k_{2,(001)}$) on (■) (101) and (▲) (001) facets of the two anatase TiO_2 catalysts, respectively (the inset graph shows the Arrhenius plots for the average rate constant k_2 for TiO_2 (101) and TiO_2 (001) catalysts, respectively).

The kinetic effects of water, a dehydration co-product and a ubiquitous component of biomass-derived oxygenates, were examined by adding water (0.05-0.5 kPa, in great excess in comparison to H_2O produced in dehydration) to the 2-propanol feed (2 kPa) at 533 K. While previous work by Rekoske et al.[30] showed that water below 1.3 kPa had no effects on 2-propanol dehydration reaction on commercial anatase TiO_2, in this work we did observe that water inhibits dehydration weakly on both TiO_2 (101) and TiO_2 (001) catalysts (Supplementary Figure 5). Under our kinetic measurements, water formed via dehydration of anhydrous 2-propanol (< 5% conversion) is never higher than 0.1 kPa. Therefore, the inhibiting effects of reactively formed water can thus be considered negligible under kinetics measurements. In kinetic analyses for rate constant determination, rate inhibition from water was not considered, and equation (1) was simplified by deleting the $K_3[H_2O]$ term from the denominator. The dependence of rate to 2-propanol dehydration can then be described by equation (2) as follows.

$$\frac{1}{r} = \frac{1}{k_2 K_1} \times \frac{1}{[C_3H_8O]} + \frac{1}{k_2} \qquad (2)$$

In principle, using equation (2) and reaction data shown in Figure 5, both the 2-propanol adsorption constants K_1 and dehydration rate constants k_2 can be calculated. However, highly reliable K_1 are only obtained at low 2-propanol partial pressures, but the rate data are much less reliable under these conditions. Therefore, the derivation of K_1 is not attempted here, and only the more reliable k_2 values are reported. By plotting $\frac{1}{r}$ versus $\frac{1}{[C_3H_8O]}$ at each temperature to obtain the intercepts, k_2 values were readily derived. For the TiO_2(101) catalyst, the rate constant k_2 increases from $0.64 \pm 0.02 \times 10^{-2}$ to $3.8 \pm 0.05 \times 10^{-2}$ s^{-1} from 503 K to 533 K, TiO_2(001) exhibits lower rate constants that increase from $0.24 \pm 0.002 \times 10^{-2}$ to $1.9 \pm 0.03 \times 10^{-2}$ s^{-1} from 503 to 533 K, as shown in the inset graph of Figure 5.

These k_2 values of TiO_2 (101) and TiO_2 (001) catalysts, however, are average rate constants of active sites on (101) and (001) facets. In order to compare the activities on (101) and (001) facets, we determined the respective rate constant on each pure facet (denoted as $k_{2,(101)}$ and $k_{2,(001)}$,

respectively), by taking into account the catalytic contribution from the minor facets on both TiO_2 catalysts (e.g., 10 % of (001) facet on TiO_2 (101) sample and 24 % of (101) facet on TiO_2 (001) sample). Detailed derivation of these rate constants is described in the Supplemental Information. The Arrhenius plots of the derived $k_{2,(101)}$ and $k_{2,(001)}$ (Figure 5) show that the activation energy for 2-propanol dehydration is much lower on (101) facet than on (001) facet (131±8 vs. 267±46 kJ mol^{-1} on (101) and (001) facets, respectively). The values of $k_{2,(101)}$ are more than 4-folds higher than $k_{2,(001)}$. The lower activity of (001) facet in comparison to (101) facet makes it difficult to reliably extract $k_{2,(001)}$ for (001) facet, leading to significant uncertainties of the determined activation energy for (001) facet. Despite of such uncertainties, the activation energy for (101) facet is consistent with that previously reported for commercial anatase TiO_2,[30] which likely contained predominantly the more thermodynamically stable (101) facet. These extracted $k_{2,(101)}$and $k_{2,(001)}$for (101) and (001) facets, together with those rate constants, i.e., k_2 for TiO_2 (101) and (001) catalysts, show a trend that the (101) facet is more reactive than (001) facet for 2-propanol dehydration under the reaction conditions studied.

DRIFTS Measurements. To provide a qualitative description of the bound species on actual TiO_2 (101) and (001) surfaces under reaction conditions for DFT calculations, DRIFTS measurements were conducted. Figure 6(a) presents DRIFTS spectra acquired at different temperatures following 2-propanol adsorption and purging on TiO_2 (101) model catalyst at 373 K using KBr as background. The spectrum of the bare TiO_2 (101) is also included; its features at 3734 and 3676/3618 cm^{-1} are ascribed to ν(OH) stretching bands for terminally bound hydroxyls and bridging hydroxyls, respectively.[32,33] The weak band at ~3500 cm^{-1} can be attributed to hydroxyls with hydrogen bonding, and the broad, a weak and broad feature centered at ~3100 cm^{-1} can be assigned to ν(OH) modes of water molecules coordinated to Ti^{4+} ions.[34] Upon 2-propanol admission at 373 K, intensities for the free –OH bands greatly diminish, either due to 2-propoxide formation via Ti-OH + C_3H_7OH = Ti-O-H_7C_3 + H_2O, and/or perturbation via hydrogen bonding between Ti-OH and 2-propanol (Ti-OH·····HO-H_7C_3). For the latter case, the ν(OH) stretching will

shift to lower frequencies, but signal intensities will maintain if there is no 2-propoxide formation via Ti-OH + C_3H_7OH = Ti-O-H_7C_3 + H_2O. The new ν(OH) band found at 3459 cm^{-1} is therefore attributed to Ti-OH perturbed by molecularly adsorbed 2-propanol. The fact that the 3459 cm^{-1} feature intensity is slightly lower than the original free hydroxyl bands indicates that both dissociative and molecular 2-propanol adsorption occur on this surface, however molecular adsorption appears to dominate. In the C-H vibrational region, the peaks at 2973, 2936 and 2873 cm^{-1} can be attributed to chemisorbed molecular 2-propanol and 2-propoxide.[35] With increasing temperature, the 3459 cm^{-1} band gradually diminishes and completely disappears at 573 K indicating continuous condensation between hydrogen-bonded Ti-OH and 2-propanol. Above ~513 K, the intensities of the free hydroxyls start to increase due to propylene desorption (Ti-O-H_7C_3 = Ti-OH + C_3H_6). By 593 K, propylene desorption completes and the original free hydroxyls completely regain their intensities. These hydroxyls are thermally stable even at 713 K. The DRIFT results indicate that under our steady-state kinetics measurement conditions (493-533 K), the (101) catalyst surface is not dry, but covered with surface hydroxyls, molecular 2-propanol, 2-propoxide, and small amount of molecular H_2O. Since adsorbed 2-propanol and 2-propoxide display identical C-H stretching vibrations, it is not possible to distinguish them based on C-H stretching vibrations. However, under the temperatures studied, intensities of Ti-OH vibrations perturbed by 2-propanol are much higher than that of the free Ti-OH vibrations, even in the absence of gas phase 2-propanol. This suggests that molecular 2-propanol is a dominant species at our kinetic measurement temperatures.

Figure 6(b) presents spectra collected on the TiO_2 (001) model catalyst. The bare sample displays three well resolved free ν(OH) bands at 3734, 3709 and 3676 cm^{-1}. The 3709 cm^{-1} band is unique for this sample, attributable to terminal –OH from the (001) facets. The broad H_2O band centered at ~3100 cm^{-1} is more intensive for this sample. In comparison to the (101) model catalyst, following 2-propanol adsorption, the (001) samples displays obvious differences worth pointing out. First, substantial amounts of free –OHs are not consumed during the adsorption step,

indicating a less active surface. Second, the perturbed band at ~3459 cm^{-1} is much weaker, indicating that 2-propanol largely adsorbs dissociatively on this surface via Ti-OH + C_3H_7OH = Ti-O-H_7C_3 + H_2O, even at 373 K. Up to a temperature of 713 K, the surface is covered with free hydroxyls and adsorbed H_2O (the broad feature centered at ~3000 cm^{-1}). It is important to note that at the temperatures of our kinetic measurements (493-533 K), the absence of perturbed Ti-OH vibrations at ~3460 cm^{-1} demonstrates the absence of molecular 2-propanol adsorption (again, in the absence of gas phase 2-propanol under the DRIFTS measurement conditions). This indicates that at these temperatures, any molecularly adsorbed 2-propanol on the non-(001) facets readily diffuses to the (001) facets to form 2-propoxide. However, this does not indicate that molecular 2-propanol must be absent on the (001) facets under kinetic measurement conditions (i.e., in the presence of gas phase 2-propanol). Nevertheless, it suggests that 2-propoxide converges are much higher on (001) facets than on (101) under the kinetic measurement conditions.

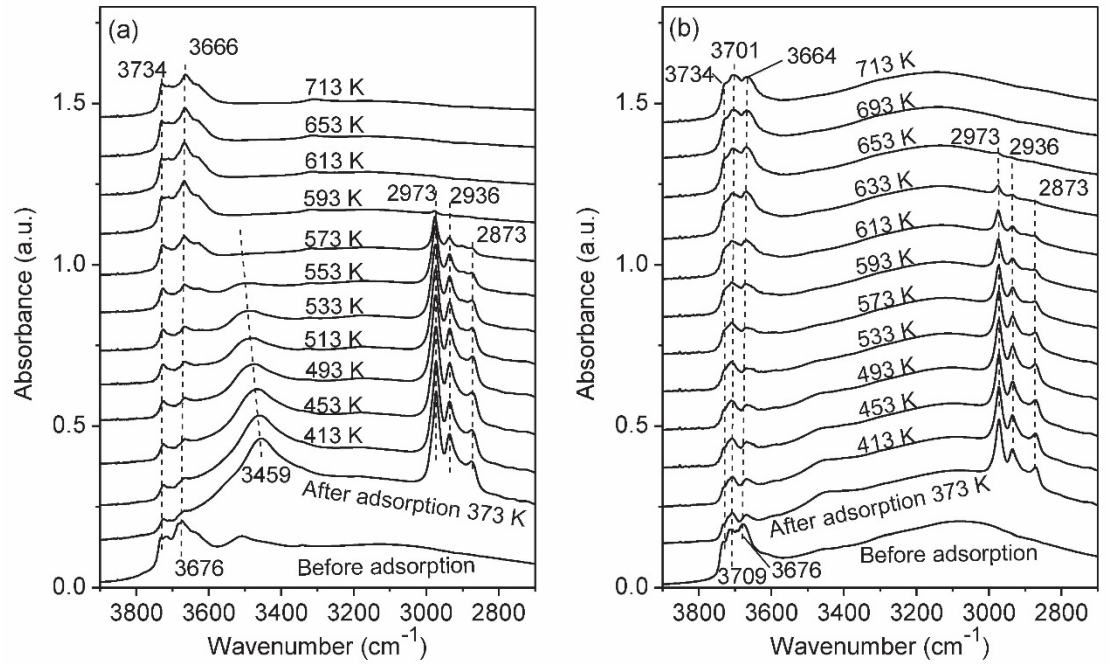

Figure 6. DRIFT spectra for TiO_2(101). DRIFT spectra acquired after 2-propanol adsorption and purging at 373 K on the (a) TiO_2 (101) and (b) TiO_2 (001) model catalyst, and then heating to

higher temperatures. Each spectrum was obtained after subtracting KBr background spectra acquired at the same temperatures.

Overall, the DRIFTS measurement results described above demonstrate considerable similarity between the two catalysts at 493-533 K. Both (101) and (001) facets are covered with surface hydroxyls and water. Note that water, particularly at low concentrations, is kinetically insignificant for 2-propanol dehydration (Supplementary Figure 5). Surface hydroxyls, on the other hand, may play important roles in catalysis, e.g., affecting surface acid-base pairs, or acting as the initial binding sites for 2-propanol adsorption. In the meanwhile, (101) and (001) facets also display important differences, i.e., 2-propanol adsorbs molecularly on (101) facets, but dissociatively on (001) facets. Kinetic data shown in Figures 4 and 5 demonstrate (101) facets are more reactive than (001) facets under reaction conditions studied. DFT calculations are thus applied in the following to elucidate mechanistic details and energetics of 2-propanol dehydration on the two facets.

DFT Calculations on Energetics of 2-Propanol Dehydration. In this section, DFT calculations of 2-propanol dehydration reaction pathways on both TiO_2(101) and (001) facets under reaction conditions studied are performed. At the onset, the rationale for the construction of working catalyst surfaces and possible mechanisms are described first. Our experimental results demonstrate that bimolecular dehydration to diisopropyl ether formation is not detectable on either anatase facet. Therefore, only unimolecular 2-propanol dehydration is considered here.

Based on DRIFTS experimental results, the initial working catalyst surfaces are constructed by introducing 7 and 8 water molecules on the dry (101) and (001) surfaces (saturation coverage), respectively. Upon relaxation, all 7 H_2O molecules dissociate on the (101) surface slab to generate 14 surface hydroxyls (7OH + 7O_sH, where O_s represents lattice oxygen). On the (101) surface, both molecular and dissociative water molecules (as two hydroxyls, OH+OsH) could be stabilized and the dissociative water molecule form is slightly more stable on the basis of static DFT

calculation results. In contrast, 7 H_2O molecules dissociate spontaneously generating 14 surface hydroxyls (7OH + 7O_sH), and 1 H_2O molecule remains intact on the (001) surface slab. The presence of 1 H_2O molecule on the (001) surface slab is largely due to repulsive lateral interaction between surface hydroxyls at high coverage conditions. Two surface hydroxyls would recombine to form one molecular water adsorbed at the Ti site. This is further confirmed by our ab initio molecular dynamics (AIMD) simulations (10 ps) in the experimental temperature range (503 K and above). Since only one 2-propanol molecule on hydroxylated (101) and (001) surfaces represents the most likely and stable situation (Supplementary Tables 1 and 2) under our working conditions, one 2-propanol molecule is subsequently introduced on the (101) and (001) surfaces, respectively, to simulate the dehydration processes. As shown in Figure 7, 2-propanol adsorbs molecularly on a 5-coordinated Ti site on the (101) surface, whereas dissociative adsorption with 2-propoxide formation is found on the (001) surface.

For the kinetically relevant dehydration step, two mechanisms, namely the E1 and E2 mechanisms, have been proposed in previous literature.[26,36] The E1 mechanism follows sequential steps, where adsorbed alcohol first undergoes C-OH cleavage to form a surface alkyl and a hydroxyl, and then the surface alkyl undergoes C-H bond scission leading to the formation of alkene. In contrast, the E2 mechanism assumes a concerted step, where both C-O and C-H bonds cleave concurrently to release gaseous alkene. Regarding the E2 mechanism, two different concerted C-H/C-O bond cleavage mechanisms are possible: H atom subtracted from an alkyl group can either bond to a surface oxygen (E2), or the oxygen from the alkanol reactant (E2'). Previous works[20,21] have shown that alcohol dehydration on anatase TiO_2 proceeds via E2 mechanism. Our DFT calculations demonstrate that E2 mechanism is energetically much more favorable than E1 mechanism; between the two E2 mechanisms, the E2 mechanism involving surface oxygen are energetically more favorable than the E2' mechanism (see Figure S9 for the results of the E2' mechanism). On the (101) surface, there is always a 2-coordinated surface oxygen available, so the E2 mechanism involves the 2-coordinated surface oxygen, rather than the

Ti_{5c}-OH site. While on the (001) surface, there is no surface oxygen available. Therefore, the E2 mechanism on the (001) surface could only involves the Ti_{5c}-OH site.

The calculated Gibbs free energies of activation for dehydration are 106 and 145 kJ/mol, respectively, for the hydroxylated (101) and (001) surfaces (Figure 7). This indicates that the hydroxylated (101) surface is intrinsically much more reactive than the hydroxylated (001) surface due to the kinetic activation barrier difference of ~39 kJ/mol. Similar trend is still held if the E2' mechanism is considered (see Figure S9 for the results of the E2' mechanism). This activity trend between the two facets from simulation is consistent with that observed experimentally.

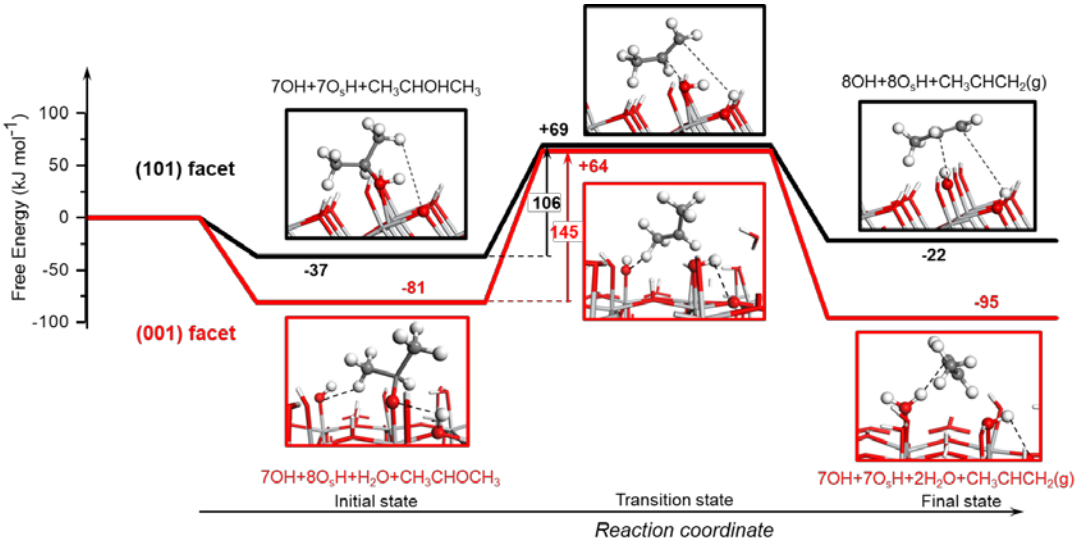

Figure 7. Free energy calculations of 2-propanol dehydration. Calculated energy profile of 2-propanol dehydration on the hydroxylated anatase TiO_2 (101) and (001) surface via the E2 mechanism (see Supplementary Figures 7 and 8 in Supplemental Information for more details of the molecular structures).

DISCUSSION

The main purpose of the present study is to investigate the faceting effect of anatase titania for alcohol dehydration. Specifically, two model catalysts with dominant (101) and (001) facets were synthesized, and their surface properties and performances were characterized and compared for 2-propanol dehydration. Acidity titration showed that the two model catalysts display sufficient differences. From the NH_3-TPD measurement, TiO_2 (101) possessed a total site density of 1.14 sites/nm^2 that was higher than TiO_2 (001) material (0.72 sites/nm^2). A parallel measurement using pyridine-IR qualitatively revealed the nature of the acidic sites: TiO_2 (101) catalyst mainly has Lewis acid sites accompanied by a small portion of Brønsted sites, while TiO_2 (001) catalyst only possesses Lewis acid sites (Table 1). This finding raised the possibility that Brønsted sites in TiO_2 (101) partially contribute to the dehydration activity, resulting in a higher rate compared to TiO_2 (001) catalyst. The titration experiments using 2,6-DBPD unambiguously demonstrated that only Lewis acid sites are active for alcohol dehydration on both TiO_2 (101) and (001) catalysts. This finding is consistent with computational studies by Kostestkyy et al.[3], who suggested that alcohol dehydration activity is dictated by the Lewis acid sites on anatase TiO_2. Vittadini et al [37]. also speculated that surface hydroxyl groups can eliminate β-hydrogens of alcohols to form either ether or alkene products.

From the activity measurements displayed in Figures 4 and 5, TiO_2 (101) exhibits higher activities and lower activation energies than TiO_2 (001) under the reaction conditions studied. DFT calculations were then used to further discern the differences between these two facets. Under our differential reaction conditions, it is first important to deduce whether the actual catalyst surfaces are partially/fully covered with 2-propanol (or 2-propoxide when 2-propanol dissociatively adsorbs) and H_2O molecules (or OH groups when H_2O dissociatively adsorbs). DRIFTS measurements shown in Figures 6 and 7 serve to qualitatively describe the surfaces under reaction conditions. Both surfaces are likely hydrated/hydroxylated under reaction, and the biggest difference in terms of 2-propanol chemisorption is that it tends to adsorb molecularly on TiO_2 (101) but maintains primarily dissociated as 2-propoxide on TiO_2 (001). With further assistance

from DFT simulations, it was found that the thermodynamically more stable 2-propoxide on TiO_2 (001) requires a much higher activation energy for E2 elimination, leading to a larger intrinsic dehydration activation barrier difference for these two model catalysts of ~39 kJ/mol. This activity trend between the two facets is consistent with that observed experimentally.

CONCLUSIONS

Two anatase titania model catalysts, with dominant exposure of (101) and (001) facets, were prepared and evaluated for 2-propanol dehydration. From rather detailed experimental studies, 2-propanol dehydration kinetic parameters were determined. Surface Lewis acid-base sites were found to be active for 2-propanol dehydration. With the aid from DRIFTS and DFT, likely working surfaces were constructed on which 2-propanol dehydration pathways were simulated. It was found that a concerted E2 elimination pathway prevails on both facets with two different initial states, i.e., molecularly adsorbed 2-prapnaol on (101) and dissociatively adsorbed 2-propoxide on (001). DFT calculation showed a higher activation energy for E2 elimination of 2-propoxide on (001) than 2-propanol on (101), which is consistent with the trend of the 2-propanol dehydration activity over the two facets observed experimentally. We demonstrate here that facet dominate model catalysts can be used to rather rigorously describe the reaction mechanisms and kinetic parameters.

ASSOCIATED CONTENT

Supplementary Information

Supplementary information is available for this paper. Additional information on DFT calculation, derivation of rate constant, characterization results of the catalysts (XRD, XPS, and Pyridine-DRIFT), impact of H_2O, and impact of addition of 2,6-DBPD were provided.

AUTHOR INFORMATION

Corresponding author

Correspondence to Huamin Wang (huamin.wang@pnnl.gov), Feng Gao (feng.gao@pnnl.gov) and Yong Wang (yong.wang@pnnl.gov)

Notes

The authors declare no competing interests.

ACKNOWLEDGEMENTS

The authors acknowledge the U.S. Department of Energy (DOE), Office of Basic Energy Sciences, Division of Chemical Sciences, Geosciences, and Biosciences for funding this project. Part of this work was conducted in the William R. Wiley Environmental Molecular Sciences Laboratory (EMSL), a national scientific user facility sponsored by DOE's Office of Biological and Environmental Research and located at Pacific Northwest National Laboratory (PNNL). PNNL is a multiprogram national laboratory operated for the DOE by Battelle. Computing time was granted by a user proposal at EMSL and the National Energy Research Scientific Computing Center

(NERSC). We also thank Prof. Enrique Iglesia from University of California at Berkeley for helpful discussions.

REFERENCES

1 Zhi, Y. *et al.* Dehydration pathways of 1-propanol on HZSM-5 in the presence and absence of water. *J. Am. Chem. Soc.* **137**, 15781-15794 (2015).

2 Zaki, T. Catalytic dehydration of ethanol using transition metal oxide catalysts. *J. Colloid. Interface Sci.* **284**, 606-613 (2005).

3 Kostestkyy, P., Yu, J., Gorte, R. J. & Mpourmpakis, G. Structure–activity relationships on metal-oxides: alcohol dehydration. *Catal. Sci. Technol* **4**, 3861-3869 (2014).

4 Lazzeri, M., Vittadini, A. & Selloni, A. Structure and energetics of stoichiometric TiO_2 anatase surfaces. *Phys. Rev. B* **63**, 155409 (2001).

5 Lazzeri, M., Vittadini, A. & Selloni, A. Structure and energetics of stoichiometric TiO_2 anatase surfaces. *Phys. Rev. B* **65**, 119901(E) (2002).

6 Yang, H. G. *et al.* Anatase TiO_2 single crystals with a large percentage of reactive facets. *Nature* **453**, 638-641 (2008).

7 Fang, W. Q., Gong, X.-Q. & Yang, H. G. On the unusual properties of anatase TiO_2 exposed by highly reactive facets. *J. Phys. Chem. Lett.* **2**, 725-734 (2011).

8 Liu, S., Yu, J. & Jaroniec, M. Anatase TiO_2 with dominant high-energy {001} facets: synthesis, properties, and applications. *Chem. Mat.* **23**, 4085-4093 (2011).

9 Gordon, T. R. *et al.* Nonaqueous synthesis of TiO_2 nanocrystals using TiF_4 to engineer morphology, oxygen vacancy concentration, and photocatalytic activity. *J. Am. Chem. Soc.* **134**, 6751-6761 (2012).

10 Liu, M. *et al.* Anatase TiO_2 single crystals with exposed {001} and {110} facets: facile synthesis and enhanced photocatalysis. *Chem. Commun.* **46**, 1664-1666 (2010).

11 Han, X., Kuang, Q., Jin, M., Xie, Z. & Zheng, L. Synthesis of titania nanosheets with a high percentage of exposed (001) facets and related photocatalytic properties. *J. Am. Chem. Soc.* **131**, 3152-3153 (2009).

12 Yu, J., Low, J., Xiao, W., Zhou, P. & Jaroniec, M. Enhanced Photocatalytic CO_2-Reduction Activity of Anatase TiO_2 by Coexposed {001} and {101} Facets. *J. Am. Chem. Soc.* **136**, 8839-8842 (2014).

13 Zhang, J. *et al.* Anatase TiO_2 nanosheets with coexposed {101} and {001} facets coupled with ultrathin SnS_2 nanosheets as a face-to-face n-p-n dual heterojunction photocatalyst for enhancing photocatalytic activity. *Applied Surface Science* **420**, 839-848 (2017).

14 Tong, H. *et al.* Anatase TiO_2 single crystals with dominant {0 0 1} facets: Synthesis, shape-control mechanism and photocatalytic activity. *Applied Surface Science* **444**, 267-275 (2018).

15 Kraemer, S. *et al.* Oxidative dehydrogenation of isobutane over vanadia catalysts supported by titania nanoshapes. *Catal. Today* **263**, 84-90 (2016).

16 Foo, G. S. *et al.* Kinetics and mechanism of methanol conversion over anatase titania nanoshapes. *ACS Catalysis* **7**, 5345-5356 (2017).

17 Wu, B., Guo, C., Zheng, N., Xie, Z. & Stucky, G. D. Nonaqueous production of nanostructured anatase with high-energy facets. *J. Am. Chem. Soc.* **130**, 17563-17567 (2008).

18 Dai, Y., Cobley, C. M., Zeng, J., Sun, Y. & Xia, Y. Synthesis of anatase TiO_2 nanocrystals with exposed {001} facets. *Nano Lett.* **9**, 2455-2459 (2009).

19 Deo, G. & Wachs, I. E. Effect of additives on the structure and reactivity of the surface vanadium oxide phase in V_2O_5/TiO_2 catalysts. *J. Catal.* **146**, 335-345 (1994).

20 Carrizosa, I. & Munuera, G. Study of the interaction of aliphatic alcohols with TiO_2: I. Decomposition of ethanol, 2-propanol, and tert-butanol on anatase. *J. Catal.* **49**, 174-188 (1977).

21 Carrizosa, I. & Munuera, G. Study of the interaction of aliphatic alcohols with TiO_2: II. On the mechanism of alcohol dehydration on anatase. *J. Catal.* **49**, 189-200 (1977).

22 Larmier, K. *et al.* Mechanistic investigation of isopropanol conversion on alumina catalysts: location of active sites for alkene/ether production. *ACS Catalysis* **5**, 4423-4437 (2015).

23 Vishwanathan, V., Roh, H.-S., Kim, J.-W. & Jun, K.-W. Surface properties and catalytic activity of TiO_2–ZrO_2 mixed oxides in dehydration of methanol to dimethyl ether. *Catal. Lett.* **96**, 23-28 (2004).

24 Manrıquez, M., López, T., Gómez, R. & Navarrete, J. Preparation of TiO_2–ZrO_2 mixed oxides with controlled acid–basic properties. *J. Mol. Catal. A-Chem.* **220**, 229-237 (2004).

25 Knaeble, W. & Iglesia, E. Kinetic and theoretical insights into the mechanism of alkanol dehydration on solid Brønsted acid catalysts. *J. Phys. Chem. C* **120**, 3371-3389 (2016).

26 Macht, J., Janik, M. J., Neurock, M. & Iglesia, E. Mechanistic consequences of composition in acid catalysis by polyoxometalate Keggin clusters. *J. Am. Chem. Soc.* **130**, 10369-10379 (2008).

27 Yang, H. G. *et al.* Solvothermal synthesis and photoreactivity of anatase TiO_2 nanosheets with dominant {001} facets. *J. Am. Chem. Soc.* **131**, 4078-4083 (2009).

28 Emeis, C. A. Determination of Integrated Molar Extinction Coefficients for Infrared Absorption Bands of Pyridine Adsorbed on Solid Acid Catalysts. *J. Catal.* **141**, 347-354 (1993).

29 Larson, S. A., Widegren, J. A. & Falconer, J. L. Transient Studies of 2-Propanol Photocatalytic Oxidation on Titania. *J. Catal.* **157**, 611-625 (1995).

30 Rekoske, J. E. & Barteau, M. A. Kinetics and Selectivity of 2-Propanol Conversion on Oxidized Anatase TiO_2. *J. Catal.* **165**, 57-72 (1997).

31 Liu, H., Bayat, N. & Iglesia, E. Site titration with organic bases during catalysis: Selectivity modifier and structural probe in methanol oxidation on Keggin clusters. *Angew. Chem. Int. Ed.* **42**, 5072-5075 (2003).

32 Finnie, K. S., Cassidy, D. J., Bartlett, J. R. & Woolfrey, J. L. IR spectroscopy of surface water and hydroxyl species on nanocrystalline TiO_2 films. *Langmuir* **17**, 816-820 (2001).

33 Erdem, B. *et al.* XPS and FTIR surface characterization of TiO_2 particles used in polymer encapsulation. *Langmuir* **17**, 2664-2669 (2001).

34 Martra, G. Lewis acid and base sites at the surface of microcrystalline TiO_2 anatase: relationships between surface morphology and chemical behaviour. *Appl. Catal., A* **200**, 275-285 (2000).

35 Zaki, M. I., Hasan, M. A. & Pasupulety, L. In situ FTIR spectroscopic study of 2-propanol adsorptive and catalytic interactions on metal-modified aluminas. *Langmuir* **17**, 4025-4034 (2001).

36 Alharbi, W., Brown, E., Kozhevnikova, E. F. & Kozhevnikov, I. V. Dehydration of ethanol over heteropoly acid catalysts in the gas phase. *J. Catal.* **319**, 174-181 (2014).

37 Vittadini, A., Selloni, A., Rotzinger, F. & Grätzel, M. Structure and energetics of water adsorbed at TiO_2 anatase (101) and (001) surfaces. *Phys. Rev. Lett.* **81**, 2954 (1998).

38 Ye, L. *et al.* Synthesis of anatase TiO_2 nanocrystals with {101}, {001} or {010} single facets of 90% level exposure and liquid-phase photocatalytic reduction and oxidation activity orders. *J. Mater. Chem. A* **1**, 10532-10537 (2013).

39 VandeVondele, J. *et al.* Quickstep: Fast and accurate density functional calculations using a mixed Gaussian and plane waves approach. *Comput. Phys. Commun.* **167**, 103-128 (2005).

40 Goedecker, S., Teter, M. & Hutter, J. Separable dual-space Gaussian pseudopotentials. *Phys. Rev. B* **54** (1996).

41 Hartwigsen, C., Goedecker, S. & Hutter, J. Relativistic separable dual-space Gaussian pseudopotentials from H to Rn. *Phys. Rev. B* **58**, 3641-3662 (1998).

42 Krack, M. & Parrinello, M. All-electron ab-initio molecular dynamics. *Phys. Chem. Chem. Phys.* **2**, 2105-2112 (2000).

43 VandeVondele, J. & Hutter, J. Gaussian basis sets for accurate calculations on molecular systems in gas and condensed phases. *J. Chem. Phys.* **127**, 114105 (2007).

44 Perdew, J. P., Burke, K. & Ernzerhof, M. Generalized gradient approximation made simple. *Phys. Rev. Lett.* **77**, 3865 (1996).

45 Zhang, Z. *et al.* OH group dynamics of 1,3-propanediol on TiO_2(110). *J. Phys. Chem. Lett.* **3**, 3257-3263 (2012).

46 Grimme, S., Antony, J., Ehrlich, S. & Krieg, H. A consistent and accurate ab initio parametrization of density functional dispersion correction (DFT-D) for the 94 elements H-Pu. *J. Chem. Phys.* **132** (2010).

47 Henkelman, G., Uberuaga, B. P. & Jonsson, H. A climbing image nudged elastic band method for finding saddle points and minimum energy paths. *J. Chem. Phys.* **113**, (2000).

48 Mills, G., Jonsson, H. & Schenter, G. K. Reversible work transition-state theory-application to dissociative adsorption of hydrogen. *Surf. Sci.* **324**, 305-337 (1995).

49 Arrouvel, C., Digne, M., Breysse, M., Toulhoat, H. & Raybaud, P. Effects of morphology on surface hydroxyl concentration: a DFT comparison of anatase-TiO_2 and gamma-alumina catalytic supports. *J. Catal.* **222**, 152-166 (2004).

50 Mei, D. & Lercher, J. A. Mechanistic insights into aqueous phase propanol dehydration in H-ZSM-5 zeolite. *AIChE J.* **63**, 172-184 (2017).

51 Song, W. *et al.* Dehydration of 1-octadecanol over H-BEA: a combined experimental and computational study. *ACS Catal.* **6**, 878-889 (2016).